

# A Janus Molecule for Screen-Printable Conductive Carbon Ink for Composites with Superior Stretchability

Peter Zalar,\* Lucia Rubino, Fatima Margani, Gerwin Kirchner, Daniele Raiteri, Maurizio Stefano Galimberti,\* and Vincenzina Barbera\*

Inspired by decades of research in the compatibilization of fillers into elastomeric composites for high-performance materials, a novel polyurethane-based stretchable carbon ink is created by taking advantage of a Janus molecule, 2-(2,5-dimethyl-1*H*-pyrrol-1-yl)propane-1,3-diol (serinol pyrrole, SP). SP is used to functionalize the carbon and comonomer in the polymer phase. The use of SPs in both the organic and inorganic phases results in an improved interaction between the two phases. When printed, the functionalized material has a factor 1.5 lower resistance-strain dependence when compared to its unfunctionalized analogue. This behavior is superior to commercially available carbon inks. To demonstrate the suitability of ink in an industrial application, an all-printed, elastomer-based force sensor is fabricated. This “pyrrole methodology” is scalable and broadly applicable, laying the foundation for the realization of printed functionalities with improved electromechanical performance.

## 1. Introduction

Printed electronics sets out to revolutionize the way that electronic circuits and components are fabricated and utilized. This is because printed electronics takes advantage of additive manufacturing methods and low-temperature processes.<sup>[1,2]</sup> In this regard, this field has already had tremendous success in realizing printed circuit boards and “components” such as thermistors, electrochemical sensors, batteries, transistors, solar

cells, and light-emitting diodes on flexible and stretchable substrates.<sup>[3–8]</sup> Futuristic concepts such as those of electronic skins, medical devices, or soft robotics will require materials with excellent flexibility and stretchability to accommodate the extreme mechanical demands to be placed on them.<sup>[9]</sup> For example, for applications related to the human body, strains of up to 50% must be accommodated.<sup>[10]</sup> This means that constituent materials, such as substrates, conductors, dielectrics, semiconductors, sensors, and encapsulants, must be carefully engineered to perform in these challenging conditions. With a toolbox of advanced materials, a mechanically compliant electronic circuit or sensor system can be readily manufactured.


Currently, most functional materials used in printed electronics consist of relatively rigid composite materials, such as those found in conductive wiring (e.g., silver pastes), dielectrics (e.g., clay composites), or sensors (e.g., force sensitive resistors).<sup>[11]</sup> Other solutions may consist of sintered metallic layers or (doped) conjugated polymers. The design of materials that possesses both the necessary electronic and mechanical performance are few, necessitating a great deal of rigorous organic synthesis and trial-and-error.<sup>[12,13]</sup> To arrive to the desired electronic and mechanical properties, the most straightforward approach is to create a printable composite consisting of a dielectric polymer phase and an inorganic filler.<sup>[14–16]</sup>

Composites are made up of two materials with different physical and chemical properties generating a “new” material with unique physical properties. In this way, one can easily imagine creating a stretchable conductive material, consisting of an electronic filler (e.g., microstructured silver or nanosized  $sp^2$  carbon allotropes) and an elastomeric polymer phase (e.g., silicone).<sup>[16–18]</sup> While this approach appears simple, various considerations must be made in order to form a homogeneous mixture of the two components. One of these factors is the chemical compatibility of the filler and polymer phases, which has a significant impact on the final properties of the material.<sup>[19,20]</sup>

To create advanced electronic composites, significant inspiration can be drawn from the polymer composites based on carbon black, such as those developed for car tires.<sup>[21]</sup> The fractal nature of the aggregates, the filler–filler network, and the surface energy all contribute to the final composite’s properties. The surface activity is essentially modified through the surface functionalization.<sup>[22–24]</sup> To create electronic composites for inks

P. Zalar, G. Kirchner, D. Raiteri<sup>[†]</sup>  
Holst Centre / TNO  
High Tech Campus 31, 5656 AE Eindhoven, The Netherlands  
E-mail: peter.zalar@tno.nl

L. Rubino, F. Margani, M. S. Galimberti, V. Barbera  
Department of Chemistry, Materials and Chemical Engineering “G. Natta”  
Politecnico di Milano  
Via Mancinelli 7, 20131 Milano, Italy  
E-mail: maurizio.galimberti@polimi.it; vincenzina.barbera@polimi.it

 The ORCID identification number(s) for the author(s) of this article can be found under <https://doi.org/10.1002/adem.202300706>.

<sup>[†]</sup>Present address: Aircision, High Tech Campus 12, 5656 AE Eindhoven, The Netherlands

© 2023 The Authors. Advanced Engineering Materials published by Wiley-VCH GmbH. This is an open access article under the terms of the Creative Commons Attribution-NonCommercial-NoDerivs License, which permits use and distribution in any medium, provided the original work is properly cited, the use is non-commercial and no modifications or adaptations are made.

DOI: 10.1002/adem.202300706

in printed electronics, this degree of attention to surface chemistries and chemical compatibility has rarely been taken. As a result, using reversible chemical interactions, a good dispersion of the conductive filler in the matrix can be achieved, allowing the carbon black to flow like beads during stretching and then return to its initial state (Figure 1).

Here, we have developed a screen-printable stretchable conductive carbon ink by taking advantage of pyrrole-functionalized carbon nanoparticles and a specifically designed pyrrole-bearing polyurethane binder. This approach reduces the impact of applied strain on the resistance on the composite when compared to an unfunctionalized system. This results in an electromechanical performance that is superior to commercially available products. These favorable qualities enable it to be used as the sensing layer in an all-printed force-sensing resistor device.

## 2. Results and Discussion

In this study, a Janus molecule was chosen and used to functionalize carbon black as well as a comonomer in the formulation of a polyurethane (PU) that forms the matrix of the carbon-based ink. The Janus molecule was 2-(2,5-dimethyl-1*H*-pyrrol-1-yl)-1,3-propanediol, also known as serinol pyrrole (SP), and its chemical structure is shown in Figure 1. SP is obtained by an innovative, green, and efficient synthetic strategy.<sup>[25,26]</sup> The use of SP facilitates the homogeneous dispersion of the carbon fillers in the polymer matrix, while having great adhesion to commonly used substrates in printed electronics, such as

thermoplastic polyurethane (TPU) and polyesters such as polyethylene terephthalate (PET) and polyethylene naphthalate (PEN). The superior properties of the ink developed and reported herein are the result of a series of supramolecular interactions. These effects stem from the use of a Janus molecule, which interacts with the polycyclic aromatic filler ( $\pi$ - $\pi$  interaction) on the one hand via the electron-rich heterocyclic ring (in the PU structure) and with the TPU support on the other via the formation of a network of hydrogen bonds (carbamate units). Furthermore, the presence of SP covalently bonded to carbon black confers polar characteristics (the diol moiety in the adduct) to the filler, allowing the formation of a further hydrogen interaction between the filler and the TPU substrate.<sup>[27–29]</sup> Figure 1 depicts the rational design.

Given that flexible electronics require a conductive filler, an adhesive, and a flexible substrate, it was decided to move on to the chemical analysis of the various components. In formulating the inks, conductive carbon black (CBc) was used either in its pristine or functionalized form with SP and a PU, with or without SP as a comonomer. The selected CBc had a high surface area, a high conductivity, and a minor amorphous part, as confirmed by wide-angle X-ray diffraction (WAXD) analysis of the pristine powder. Further analysis of the CBc is detailed in the Supporting Information (SI).

It has been shown that  $sp^2$  carbon allotropes can be functionalized with pyrrole compounds mainly in peripheral positions, essentially on the edges of graphene-like layers.<sup>[30]</sup> In this case, a domino reaction occurs: the carbocatalyzed oxidation of the pyrrole compound followed by a Diels–Alder cycloaddition which

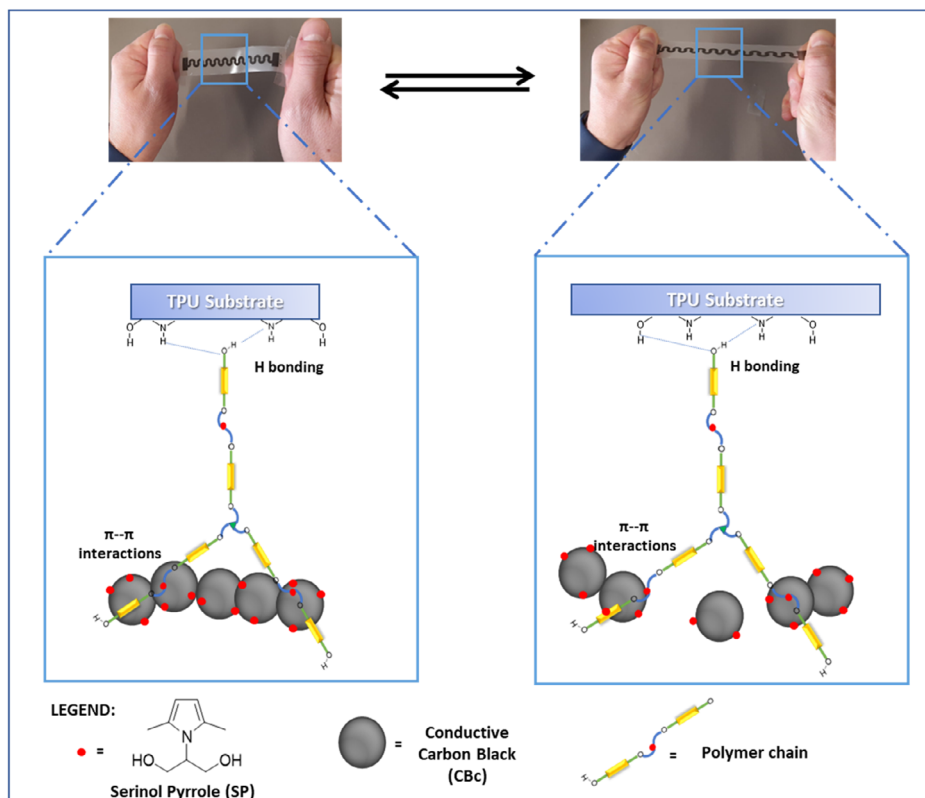


Figure 1. Rationale: insight into the chemical interaction of the innovative ink with the TPU-substrate.

leads to covalent functionalization. This “pyrrole method” is selected since it allows for the fine tuning of the chemical surface properties of the  $sp^2$  carbon allotropes by putting functional groups on their surface.<sup>[31]</sup> The type and amount of these functional groups are crucial for changing the surface’s properties. Achieving desired functionalities by increasing the surface energy improves the compatibility of the matrix and the filler. Indeed, it was reported that the solubility parameters of a  $sp^2$  carbon allotrope could be tuned by means of the functionalization with pyrrole compounds, synthesized through the reaction of an ad hoc primary amine with a diketone.<sup>[32,33]</sup>

In this work, the correct pyrrole compound was selected considering that the good one has a chemical structure in which there are functional groups capable of giving step-growth polymers and conferring polar properties to the filler. The Janus molecule (SP), which has previously been described, was chosen.<sup>[25]</sup>

The Paal–Knorr reaction of serinol with 2,5-hexanedione yielded SP.<sup>[25]</sup> The synthesis was performed in the absence of solvents and catalyzes, simply by mixing and heating the reagents, with water as the only coproduct, and was characterized by very high yield and thus high atom efficiency. The synthesis and characterizations of SP are reported in the Supporting Information (Figure S1–S3). The pyrrole compound (SP) was thus used, without any purification, for the preparation of the adducts with carbon black (CBc). In brief, CBc-SP adducts were prepared by simply mixing the carbon allotrope and SP and giving thermal energy (heat) to drive the reaction. Adducts between CBc and SP were prepared using an amount of SP of 1 and 5 considering 100 parts of carbon (per hundred carbon, phc). The covalent adducts obtained were labeled as CBc-SP1 and CBc-SP5, respectively. Further details are in the Experimental Section and Supporting Information (S2).

The adhesive was prepared taking into consideration both the chemical characteristics of the substrate and the polycyclic aromatic nature of the filler. It was decided to synthesize a polyurethane-based adhesive on the basis of what was already reported by some of the authors about the ability of SP-based PU on to supramolecular adducts with  $sp^2$  carbon allotropes.<sup>[27–29]</sup> The preparation of PU bearing the SP comonomer ( $PU_{SP}$ ) was performed starting from a mixture of polyols, a polyether polyol (PPG-PEG-PPG), 1,4-butanediol, SP, with glycerol as the branching molecule. The isocyanate was 1,6-hexamethylene diisocyanate (HDI). In addition, a reference PU was prepared, using only 1,4-butanediol ( $PU_{BOH}$ ) as the chain extender. The reaction schemes for the synthesis of  $PU_{SP}$  and  $PU_{BOH}$  are in the Supporting Information (S3, Scheme S1 and S2). The substitution of an aliphatic diol with the one substituted with a heterocycle does not significantly alter how the chains interact, since the thermal behavior of the two polymers is fairly comparable (Figure S11, Supporting Information). The polymer based on 1,4-butanediol is insoluble, whereas the one with SP is soluble in both protic and aprotic polar solvents, suggesting that the heterocycle only seems to improve its solubility characteristics.

With these building blocks, namely, CBc, CBc-SP,  $PU_{SP}$ , and  $PU_{BOH}$ , inks suitable for screen printing can be formulated. First, CBc or CBc-SP is dispersed in a mixture of propylene glycol and 2-butoxyethanol (hereafter referred to as “pre-Ink”). It was decided to use 2-butoxyethanol due to its volatility and propylene glycol due to its miscibility in a wide range of solvents. The

composition of all the pre-inks is in the supporting information (S4, Table S4, Supporting Information). The dispersions were characterized by high-resolution transmission electron microscopy (HRTEM), revealing the presence of carbon aggregates made up of spherical particles with an average size of about 30 nm (S4, Figure S13, Supporting Information). From these micrographs, it can be seen that a better filler distribution was provided for CBcSP5 and CBcSP1 when compared with unfunctionalized and commercially available carbon ink. This aspect seems crucial for obtaining a better interaction between filler particles and the polyurethane adhesive matrix in the final ink. In fact, a premix without agglomerates will provide a greater surface area for the interaction between the polyurethane and the filler. At higher magnifications, the presence of highly disordered graphitic particles and primary particles with a porous structure is observed. Importantly, it appears that the SP functionalization process did not cause morphological changes of the aggregates.

To obtain screen-printable inks, pre-ink dispersions were blended with  $PU_{SP}$  or  $PU_{BOH}$  using a planetary mixer. By adjusting the ratio of the carbon filler and the PU phase, the conductivity of the resultant ink can be tuned according to the needs of the final application. Homogeneous mixtures of CBc and CBc-SP are obtained only with the  $PU_{SP}$  polymer as confirmed by transmission electron microscopies (Figure S15, Supporting Information). A blend of  $PU_{BOH}$  with CBc yields undispersed carbon. This mixture is characterized by insoluble macroaggregates in both polar and apolar solvents. This finding indicates the key role of the pyrrole ring in the PU chain in facilitating an even dispersion of the carbon particles. As a result, inks tested for screen printing were thus prepared with  $PU_{SP}$  and either CBc, CBc-SP1, or CBc-SP5, as reported in the supporting information (S4, Table S5, Supporting Information) These inks are hereafter referred to as  $INK_{CB}$ ,  $INK_{CB-SP1}$ , and  $INK_{CB-SP5}$ , respectively.

The TEM and HRTEM micrographs of the inks prepared in this work and a commercial ink ( $INK_{COMM}$ , Dupont PE671) are shown in Supporting Information (S4, Figure S15, Supporting Information), while TEM and HRTEM micrographs of  $INK_{CB-SP1}$  at low and high magnification are reported in **Figure 2**.

Analysis of micrographs of the commercial ink reveals that the polymer phase appears to interact in a limited way with carbon. In fact, isolated polymeric materials were detected (S4 Figure S15, Supporting Information). In the case of CBc or CBc-SP-based inks, the differences seem enormous. Inspection of the micrographs in Figure 2 and S15, Supporting Information, reveals the presence of polymeric material adhered to the carbonaceous structures functionalized with SP (indicated by red arrows), while if unfunctionalized CBc was used as the filler, agglomerates of polymeric material were detected (red arrow in Figure S15c, Supporting Information). The nature of this interaction is currently under investigation.

In order to compare their electronic performance under strain, the inks were screen printed atop stretchable TPU substrates (S4, Figure S16, Supporting Information). All inks were cured at 110 °C for 30 min and the thickness of all layers, as determined by the mesh size of the screen used for printing, was measured to be  $\approx 8 \mu\text{m}$  by profilometry.

Scanning electron microscopy (SEM) images of the printed traces are shown in Figure 2. The topological investigation performed on the substrates reveals that the TPU (Figure 2Aa)

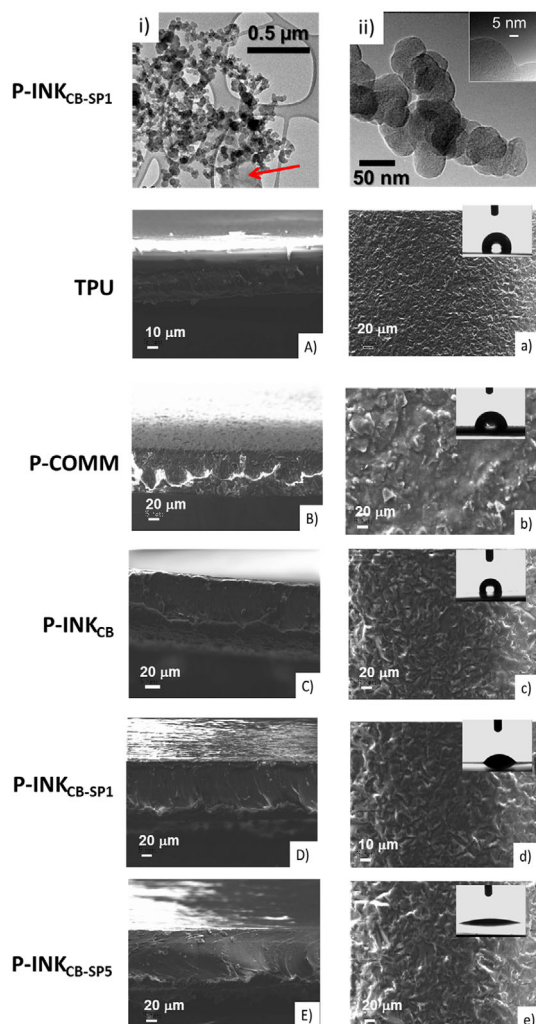


**Figure 2.** TEM and HRTEM micrographs of Ink<sub>CB-SP1</sub> at low (i) and high magnification (ii). The inset shows that the particles' fine structure remains intact after functionalization. SEM micrographs of aA) the TPU film as received, bB) P-COMM; cC) P-INK<sub>CB</sub>; dD) P-INK<sub>CB-SP1</sub>; and eE) P-INK<sub>CB-SP5</sub>, visualizing cross sections (A–E) and the surfaces (a–e). Corresponding contact angle measurements are shown in the insets of each pair (a–e).

substrate is characterized by a rough surface. Analyzing the cross sections of the printed substrates (Figure 2B–E), it appears that the cured commercial ink is an irregular, grainy, and opaque layer that appears to adhere to the substrate, modifying its structure (Figure 2B). This irregular stratification suggests an ink penetration process into the substrate during printing or curing.

Morphologies of the printed substrates obtained using inks based on PU<sub>SP</sub> as the binder show a progressive reduction of roughness, indicating that the interactions between the substrate, the polyurethane, and the carbon improve as the polarity of the carbon changes (Figure 2C–E). Contact angles were also measured; insets in Figure 2 show that the TPU substrate (103°), the commercial ink and INK<sub>CB</sub> (105°), are strongly hydrophobic while INK<sub>CB-SP1</sub> (38°) and INK<sub>CB-SP5</sub> (31°) are hydrophilic.

The surface energies of printed layers are tunable due to the functionalization of the filler and polymer.

Conductive layers can be readily utilized as strain sensors, by monitoring the change in resistance as a function of tensile or compressive strain.

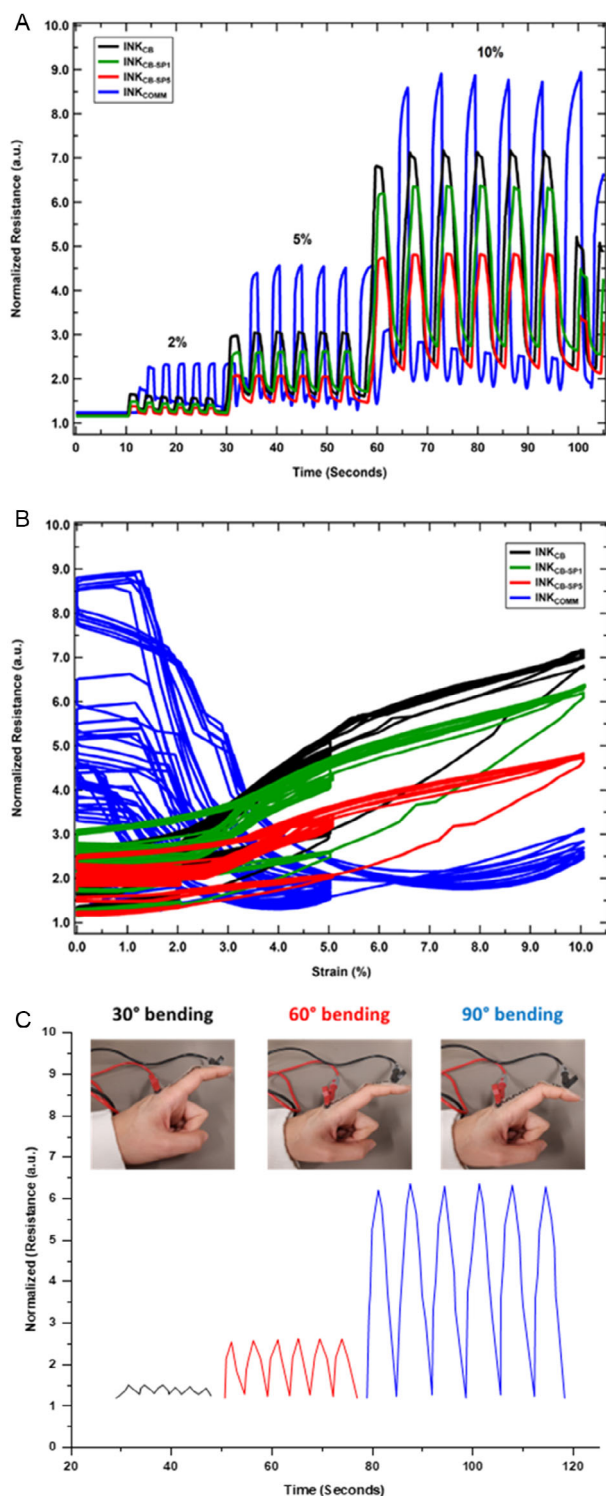
Systematic evaluation of printed samples for their electromechanical properties was performed using a tensile tester coupled with a four-point resistance measurement setup. In order to compare different inks, each sample's starting resistance is normalized to 1, and they are stretched according to the method described in the Supporting Information, which consists of six cycles up to progressively higher strain levels (2%, 5%, 10%) at a strain rate of  $\approx 4.4\% \text{ s}^{-1}$  (S4, Table S6, Supporting Information). The initial resistance of the different printed inks in this configuration is 2.38, 1.84, 3.05, and 3.29 M $\Omega$  for INK<sub>COMM</sub>, INK<sub>CB</sub>, INK<sub>CB-SP1</sub>, and INK<sub>CB-SP5</sub>, respectively. The gradual increase in initial resistance as a function of the degree of functionalization agrees with the notion that functional groups allow for a better dispersion of the filler in the polymer matrix, reducing filler–filler interaction. This has been observed in the past for bionanocomposites based on graphene layers functionalized with SP.<sup>[33]</sup>

Figure 3A shows the resistance changes as a result of applying various strain levels, as described above. Figure 3B, shows the resistance–strain curves of all the studied inks. The test shown here is similar to that of a ‘strain gauge’, whereby in the ideal case the resistance should increase geometrically.<sup>[34]</sup> In practice, purely geometric increases in resistance are rare or occur only in very-low-strain regimes. In our measurements, the baseline (resistance at 0% strain) of each sample increases due to the residual strain of the TPU substrate. The residual strain of the substrate was calculated to be  $\approx 4\%$ .

The resistance–strain curve of INK<sub>COMM</sub> shows a peculiar dependence, with the maximum resistance being measured at the lowest strain levels. In other words, the peak resistance occurs when no strain is applied to the sample. This out-of-phase behavior is likely caused by the extremely slow mechanical relaxation of the polymer matrix caused by poor interaction of the filler with it. In contrast, INK<sub>CB</sub>, INK<sub>CB-SP1</sub>, and INK<sub>CB-SP5</sub> have a much more conventional behavior. However, what is important, and key to our approach is the fact that the introduction of progressively more SP functionalization effectively helps to minimize the overall change in the resistance–strain curve (Figure 3B) by significantly reducing hysteresis and resistance changes. The maximum resistance changes for INK<sub>CB</sub>, INK<sub>CB-SP1</sub>, and INK<sub>CB-SP5</sub> are respectively factors of 7.1, 6.4, and 4.7 more than the starting resistance. This exemplifies the benefits of the synergy created between SP-functionalized CB and the SP-functionalized PU.

The screen-printed ink's electromechanical response was performed by attaching a printed trace of P-INK<sub>CB-SP1</sub> to the index finger. As the finger is bent, the tensile strain is applied to the sensor, resulting in an increase of the resistance. Figure 3C shows the response of the strain sensor, with the finger being bent 30°, 60°, and 90°. All of the results above provide a preliminary indication of the sensor's ability to monitor various human body deformations and could meet the needs of a wide range of robotic or human–machine systems in the fields of artificial intelligence.





**Figure 3.** A) Normalized resistance for INK<sub>CB</sub> (black), INK<sub>CB-SP1</sub> (green), and INK<sub>CB-SP5</sub> (red) in comparison to INK<sub>COMM</sub> (blue) as a function of time at annotated levels of strain. B) Normalized resistance for INK<sub>CB</sub> (black), INK<sub>CB-SP1</sub> (green), and INK<sub>CB-SP5</sub> (red) in comparison to INK<sub>COMM</sub> (blue) as a function of strain. C) Resistance responses of the INK<sub>CB-SP1</sub> printed on the TPU substrate; the inset shows the finger motion (bending of 30°, 60°, and 90°) and photographs of the wearable sensor.

To demonstrate the feasibility of utilizing the developed ink in a real-world printed electronic device, it was decided to implement INK<sub>CB-SP5</sub> in an all-screen-printed force sensor, a device we have previously demonstrated.<sup>[35,36]</sup> This type of device created using printed electronics and similar devices can already be purchased commercially.<sup>[37,38]</sup> These sensors are used in fields like robotics (tactile sensing), automotive (passenger detection), and sports (smart socks).<sup>[39–42]</sup> The force sensor takes advantage of a 3D structure where the top foil bearing the carbon film progressively increases its contact with the bottom foil bearing interdigitated Ag electrodes. The carbon layer should have electronic properties that are mechanically reversible and minimally affected under strain, a requirement filled by the SP functionalized ink. In this sensor, the initial measured resistance is infinite and decreases with applied force. The dynamic range and sensitivity of the sensors can be adjusted by modifying the geometrical width/length (W/L) ratio of the space between the bottom electrodes, changing the spacer height, or by selecting substrates with different mechanical properties. The cross section of the sensor is schematically shown in the inset reported in Figure 4A.

In our demonstration, the force sensor was built using TPU for the top and bottom foil. Details on its construction are found in the Experimental Section. A picture of a screen-printed pressure sensor array is in Figure 4B. Force was delivered to the sensor from the carbon side using a tensile tester while the resistance of the sensor was recorded.

In the sensor characteristics shown in Figure 4A, the resistance has an exponential-like dependence as more pressure is applied, reaching a minimum value that is dictated by the resistance of the carbon layer. In this case, at 20 kPa, a minimum resistance of  $\approx 1.3$  k $\Omega$  is measured. Ideal sensors exhibit no hysteresis when force is applied and released. In this demonstration, the hysteresis is minimized due to the excellent mechanical properties of the carbon. The maximum hysteresis is observed in the highest-sensitivity region of the sensor (0–3 kPa) and may also arise from nonelastic deformation of the top substrate.

### 3. Conclusion

A Janus molecule such as SP, characterized by a double face like the ancient Roman God, Giano, succeeds in interacting both with the matrix and the conductive filler: 1) with the diol moiety (one face), it behaves as a monomer in a polymer, while providing a pyrrole ring (second face), which is able to interact with the filler; and 2) it reacts with the carbon surface with the heterocyclic moiety (one face) and leaves the diol (second face) to interact with the matrix by hydrogen bonding. Thanks to this double nature, it has allowed for a novel approach in the creation of highly stretchable PU-based carbon inks with excellent electromechanical properties. The conductivity of the carbon inks can be tuned by adjusting the carbon loading. Much like other elastomeric composites, like car tires, we have also identified the importance of polymer-filler chemical compatibility in electronic inks. The degree of SP functionalization on the carbon significantly influences the resistance–strain behavior of printed inks, mainly due to the progressively improved compatibility with the SP-based PU polymer phase. This simple yet powerful approach is applicable to other

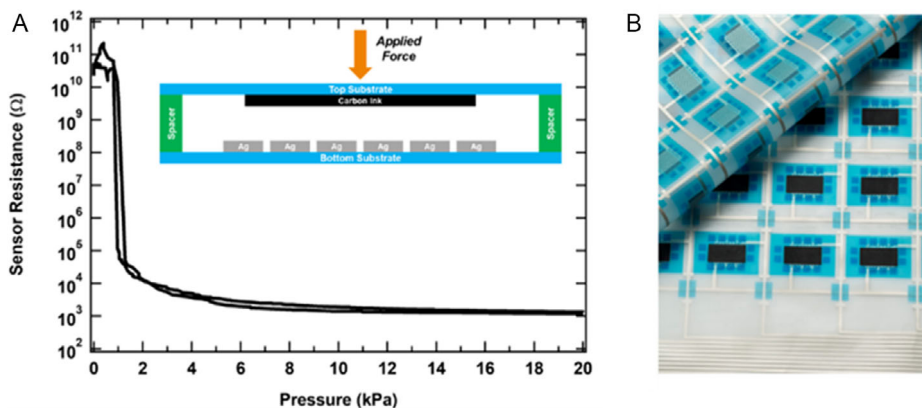


**Figure 4.** A) Resistance–pressure characteristics for force sensitive resistors based on the developed ink. The inset of the plot shows a schematic illustrating a cross section of the force-sensitive resistor device studied. B) A picture of a screen-printed pressure sensor array.

inorganic fillers and should enable the creation of highly stretchable electronic inks that can meet the ambitious targets demanded by futuristic electronic device concepts. As a result of what has been reported, it is possible to assert that this study qualifies as a technology, as it exhibits all of the characteristics of an easily scalable system on at least a pre-industrial scale.<sup>[43]</sup>

## 4. Experimental Section

**Materials:** Serinol was kindly provided by Bracco. 2,5-hexanedione, Poly(propylene glycol)-block-poly(ethylene glycol)-block-poly(propylene glycol) (PPG-PEG-PPG, Mn ≈ 2.000), 1,4-butanediol, glycerol, 1,6-hexamethylene diisocyanate (HDI), propylene glycol, 2-butoxyethanol were purchased from Sigma-Aldrich. CBc was ENSACO 360G from Imerys (30 nm as mean diameter of spherical primary particles, BET surface area 780 m<sup>2</sup> g<sup>-1</sup>, and volume resistivity 19 Ohm × cm). 2-(2,5-dimethyl-1H-pyrrol-1-yl)propan-1,3-diol (Serinol pyrrole, SP) was prepared as reported by Barbera et al.<sup>[13]</sup> and in S1, Supporting Information. A commercially available ink was selected as comparison in order to check the performances of innovative INKs: a stretchable carbon conductor paste for printed low-voltage circuitry on elastic film and textile substrates (DUPONT INTEXAR PE671). The commercial ink was made up of two components: the carbon conductor (Dupont PE671) and the adhesive stretchable (Dupont PE773).

**Synthesis of 2-(2,5-Dimethyl-1H-Pyrrol-1-Yl)-1,3-Propanediol (Serinol Pyrrole, SP):** The synthesis of 2-(2,5-dimethyl-1H-pyrrol-1-yl)-1,3-propanediol (serinol pyrrole, SP) (S1, Supporting Information) was performed by reacting an equimolar amount of 2-amino-1,3-propanediol (Serinol, S) with 2,5-hexanedione (HD), at 155 °C for 3 h. Figure S1, Supporting Information reports the reaction pathway for the synthesis of SP. At the end of the reaction, the product was obtained with a yield of 97% and was analyzed by means of NMR spectroscopy. (S1, Figure S2, Supporting Information)

**Carbon Functionalization:** The carbon allotrope (Imerys Ensaco 360G, 10 g) and acetone (Carlo Erba, 200 mL) were added to a round-bottomed flask. The mixture was sonicated in an ultrasonic bath for 15 min. In a separate flask, a solution of serinol pyrrole (prepared as reported in S2, Supporting Information, 0.1 g for CBc-SP 1 phc, or 1 g for CBc-SP 5 phc) was added to the carbon suspension and sonicated for 15 min. After this, the solvent was removed by rotary evaporation to yield a carbon/serinol pyrrole powder, which was stirred at 180 °C for 2 h. The mixture was then cooled to room temperature and vigorously washed with acetone. The final powder was obtained by vacuum filtration. The degree

of functionalization was determined by means of TGA. (Figure S5, Supporting Information)

**Polymer Synthesis:** The polymerization of polyurethane was performed starting from a mixture of polyols, containing a polyether polyol (PPG-PEG-PPG, Sigma Aldrich, 90 g), 1,4-butanediol (Sigma Aldrich, 16.22 g), serinol pyrrole (S1, Supporting Information, 30.42 g), and glycerol (Sigma Aldrich, 4.14 g) as the branching molecule. 1,6-hexamethylene diisocyanate (HDI, Sigma Aldrich, 68.1 g) was used as the isocyanate. The polyol, glycerol, and the chain extenders were mixed at room temperature for 5 min. After this time, the isocyanate was added, and the reaction was left to stir for 12 h. Then, an excess of isocyanate and 20 mL of 2-butoxyethanol were added. The composition and recipes for the preparation of PU adhesives are reported in Table S3, Supporting Information. A reference PU was prepared, with only 1,4-butandiol (PUBOH) as the chain extender. The reaction schemes for the synthesis of PUSP and PUBOH are reported in S3, Schemes S1 and S2, Supporting Information, respectively.

**Ink Preparation:** In a beaker equipped with a magnetic stirrer, carbon allotrope (10 g, unfunctionalized, 1 phc, or 10 phc) was added together with propylene glycol (Aldrich, 19.3 mL) and 2-butoxyethanol (200 mL). The mixture was left stirred for 24 h at room temperature. To from the screen-printable ink, a part of this mixture (≈17.8 g) was blended together with the polymer phase (≈20 g) and homogenized in a planetary mixer at 2000 rpm for 2 min. The viscosity of the ink was modified according to environmental conditions by adding small amounts of 2-butoxyethanol. By adjusting the mass ratio of the polymer phase and the carbon mixture, the conductivity and viscosity of the final screen-printed ink can be modified.

**Characterization:** <sup>1</sup>H-NMR and <sup>13</sup>C-NMR spectra were recorded on a Bruker 400 MHz (100 MHz <sup>13</sup>C) instrument at 298 K. Chemical shifts were reported in ppm with the solvent residual peak as internal standard (DMSO-*d*<sub>6</sub>: δH = 2.50 ppm, CDCl<sub>3</sub>: δH = 7.26 ppm).

TGA tests under flowing N<sub>2</sub> (60 mL min<sup>-1</sup>) were performed with a Perkin Elmer STA 6000 instrument according to the standard method ISO9924-1. Method used for adducts with CBc: samples (5–10 mg) were heated from 30 to 300 °C at 10 °C min<sup>-1</sup>, kept at 300 °C for 10 min, and then heated up to 550 °C at 20 °C min<sup>-1</sup>. After being maintained at 550 °C for 15 min, they were further heated up to 900 °C with a heating rate of 10 °C min<sup>-1</sup> and kept at 900 °C for 3 min and then kept at 900 °C for 30 min under flowing air (60 mL min<sup>-1</sup>). The IR spectra were recorded in transmission mode (128 scan and 4 cm<sup>-1</sup> resolution) in a diamond anvil cell (DAC) using a ThermoElectron FTIR Continuum IR microscope. WAXD patterns were obtained in reflection, with an automatic Bruker D8 Advance diffractometer, with nickel-filtered Cu Kα radiation. Patterns were recorded in 10°–90° as the 2θ range, 2θ the peak diffraction angle. Distance between crystallographic planes was calculated from the Bragg law. The Dhkl correlation length, in the direction perpendicular to the hkl crystal

graphitic planes, was determined applying the Scherrer equation  $D_{hkl} = K \lambda / (\beta_{hkl} \cos \theta_{hkl})$ , where  $K$  is the Scherrer constant,  $\lambda$  is the wavelength of the irradiating beam (1.5419 Å, Cu-K $\alpha$ ),  $\beta_{hkl}$  is the width at half height, and  $\theta_{hkl}$  is the diffraction angle. The instrumental broadening,  $b$ , was determined by obtaining a WAXD pattern of a standard silicon powder 325 mesh (99%), under the same experimental conditions. The width at half height,  $\beta_{hkl} = (\beta_{hkl} - b)$ , was corrected, for each observed reflection with  $\beta_{hkl} < 1^\circ$ , by subtracting the instrumental broadening of the closest silicon reflection from the experimental width at half height,  $\beta_{hkl}$ . HRTEM investigations on CBc samples taken from the sonicated suspensions were carried out with a Philips CM 200 field-emission gun microscope operating at an accelerating voltage of 200 kV. Few drops of the suspensions were deposited on 200 mesh lacey carbon-coated copper grid and air dried for several hours before analysis. During acquisition of HRTEM images, the samples did not undergo structural transformation. Low-beam current densities and short acquisition times were adopted.

**Samples for Tensile Testing:** All layers were screen printed onto  $\approx 90$   $\mu$ m-thick TPU substrates (DuPont, Intexar, TE-11C) using a Dek Horizon 03i screen printer. After printing, the layers were dried at 110 °C for 30 min in a box oven. The layer thickness of printed traces was on the order of 6–8  $\mu$ m, which was mainly dictated by the screen and the solid content of the ink.

**Force-Sensitive Resistor:** Similar to the samples for tensile testing, all layers were screen printed onto  $\approx 90$   $\mu$ m-thick TPU substrates (DuPont, Intexar, TE-11C) using a Dek Horizon 03i screen printer. The bottom foil consisted of printed Ag ( $\approx 8$   $\mu$ m, DuPont 5025 Silver Conductor) and a spacer layer ( $\approx 24$   $\mu$ m, DuPont 5018 UV Curable Dielectric). The Ag layer was cured in a box oven at 120 °C for 10 min and the spacer was cured in a UV box at an energy density of 500–1500 mJ cm $^{-2}$ . The top foil consisted of INKCB-SP5, processed using the same conditions for the tensile testing samples or the commercially available carbon (INKCOMM, DuPont PE773), cured at 110 °C for 10 min. To finish the sensor, as schematically shown in Figure 4A (insert), the top and bottom foils were laminated to one another with a hot press at 100 °C for 2 min. The sensor was characterized in a tensile tester (Mark-10 ESM303) by pushing on the top foil while recording the force. The resistance of the sensor was simultaneously measured using a source-measure unit (Keithley 2612A).

**Material & Film Characterization:** The powders were characterized by means of thermogravimetric analysis (TGA), infrared spectroscopy, X-ray diffraction, and HRTEM (details are as supplementary materials). Contact angle measurements and SEM were performed on printed substrates: the contact angle instrument was a Data Physics OCA 150, and the software was SCA20 version 2.3.9. build 46. The contact angles were measured directly on the printed ink surface, putting above water droplets of 2  $\mu$ L; SEM images were obtained using a Zeiss Evo 50 EP SEM with an operating voltage of 15 kV.

**Electrical & Mechanical Characterization:** Tensile tests were performed using a Mark-10 tensile tester coupled with a Keithley 2612A, for four-point resistance measurements. Electrical contact to the measurement setup was made by clamping the samples onto a Cu electrode. To compare the studied ink with the state-of-the-art stretchable ink, DuPont Intexar PE671 was chosen as a benchmark; the conductivity was adjusted by mixing it with DuPont Intexar PE773. Samples were loaded and unloaded using the methods reported in Table S6, found in the Supporting Information.

## Supporting Information

Supporting Information is available from the Wiley Online Library or from the author.

## Acknowledgements

P.Z. and L.R. contributed equally to this work. This work was supported by the Electronic Components and Systems for European Leadership Joint Undertaking (ECSEL JU) in collaboration with the European Union's

H2020 framework program (H2020/2014-2020), under grant agreement H2020-ECSEL-2019-IA-876190 “Moore4Medical”.

## Conflict of Interest

The authors declare no conflict of interest.

## Data Availability Statement

The data that support the findings of this study are available from the corresponding author upon reasonable request.

## Keywords

electronic inks, polyurethane binders, printed electronics, pyrrole methodology,  $sp^2$  carbon allotropes, sustainable functionalization

Received: May 31, 2023

Published online:

- [1] B.-H. Lu, H.-B. Lan, H.-Z. Liu, *Opto-Electron. Adv.* **2018**, *1*, 17000401.
- [2] G. Liu, X. Zhang, X. Chen, Y. He, L. Cheng, M. Huo, J. Yin, F. Hao, S. Chen, P. Wang, S. Yi, L. Wan, Z. Mao, Z. Chen, X. Wang, Z. Cao, J. Lu, *Mater. Sci. Eng., R* **2021**, *145*, 100596.
- [3] Y. Khan, A. Thielens, S. Muin, J. Ting, C. Baumbauer, A. C. Arias, *Adv. Mater.* **2020**, *32*, 1905279.
- [4] T. Yokota, P. Zalar, M. Kaltenbrunner, H. Jinno, N. Matsuhisa, H. Kitanosako, Y. Tachibana, W. Yukita, M. Koizumi, T. Someya, *Sci. Adv.* **2016**, *2*, 1501856.
- [5] S. Niu, N. Matsuhisa, L. Beker, J. Li, S. Wang, J. Wang, Y. Jiang, X. Yan, Y. Yun, W. Burnett, A. S. Y. Poon, J. B. H. Tok, X. Chen, Z. Bao, *Nat. Electron.* **2019**, *2*, 361.
- [6] M. S. White, M. Kaltenbrunner, E. D. Głowacki, K. Gutnichenko, G. Kettlgruber, I. Graz, S. Aazou, C. Ulbricht, D. A. M. Egbe, M. C. Miron, Z. Major, M. C. Scharber, T. Sekitani, T. Someya, S. Bauer, N. S. Sariciftci, *Nat. Photonics* **2013**, *7*, 811.
- [7] A. M. Gaikwad, B. V. Khau, G. Davies, B. Hertzberg, D. A. Steingart, A. C. Arias, *Adv. Energy Mater.* **2015**, *5*, 1401389.
- [8] M. Kaltenbrunner, M. S. White, E. D. Głowacki, T. Sekitani, T. Someya, N. S. Sariciftci, S. Bauer, *Nat. Commun.* **2012**, *3*, 770.
- [9] S. Peng, S. Wu, Y. Yu, B. Xia, N. H. Lovell, C. H. Wang, *ACS Appl. Mater. Interfaces* **2020**, *12*, 22179.
- [10] Y. Menguc, Y.-L. Park, H. Pei, D. Vogt, P. M. Aubin, E. Winchell, L. Fluke, L. Stirling, R. J. Wood, C. J. Walsh, *Int. J. Rob. Res.* **2014**, *33*, 1748.
- [11] T. C. Shyu, P. F. Damasceno, P. M. Dodd, A. Lamoureux, L. Xu, M. Shlian, M. Shtein, S. C. Glotzer, N. A. Kotov, *Nat. Mater.* **2015**, *14*, 785.
- [12] W. Li, Q. Sun, L. Li, J. Jiu, X.-Y. Liu, M. Kanehara, T. Minari, K. Suganuma, *Appl. Mater. Today* **2020**, *18*, 100451.
- [13] C.-Y. Yang, M.-A. Stoeckel, T.-P. Ruoko, H.-Y. Wu, X. Liu, N. B. Kolhe, Z. Wu, Y. Puttisong, C. Musumeci, M. Massetti, H. Sun, K. Xu, D. Tu, W. M. Chen, H. Y. Woo, M. Fahlman, S. A. Jenekhe, M. Berggren, S. Fabiano, *Nat. Commun.* **2021**, *12*, 2354.
- [14] S. Huang, Y. Liu, Y. Zhao, Z. Ren, C. F. Guo, *Adv. Funct. Mater.* **2019**, *29*, 1805924.
- [15] J. Kwon, C. DelRe, P. Kang, A. Hall, D. Arnold, I. Jayapura, L. Ma, M. Michalek, R. O. Ritchie, T. Xu, *Adv. Mater.* **2022**, *34*, 2202177.

- [16] A. Mohammed, M. Pecht, *Appl. Phys. Lett.* **2016**, *109*, 184101.
- [17] N. Matsuhisa, M. Kaltenbrunner, T. Yokota, H. Jinno, K. Kuribara, T. Sekitani, T. Someya, *Nat. Commun.* **2015**, *6*, 7461.
- [18] N. Matsuhisa, D. Inoue, P. Zalar, H. Jin, Y. Matsuba, A. Itoh, T. Yokota, D. Hashizume, T. Someya, *Nat. Mater.* **2017**, *16*, 834.
- [19] M. Galimberti, V. Barbera, A. Sironi, in *High-Performance Elastomeric Materials Reinforced By Nano-Carbons* (Eds: L. Valentini, M. A. Lopez Manchado), Elsevier **2020**, Ch. 3, pp. 43–92, <https://link.springer.com/book/9781851668649>.
- [20] S. Guerra, V. Barbera, U. Giese, M. Galimberti, *Kautsch. Gummi Kunstst.* **2020**, *4*, 17.
- [21] R. Muramatsu, H. Takahashi, *Int. Polym. Sci. Technol.* **2001**, *28*, 47.
- [22] M. Galimberti, G. Infortuna, S. Guerra, V. Barbera, S. Agnelli, S. Pandini, *Express Polym. Lett.* **2018**, *12*, 265.
- [23] S. Agnelli, S. Pandini, F. Torricelli, P. Romele, A. Serafini, V. Barbera, M. Galimberti, *Express Polym. Lett.* **2018**, *12*, 713.
- [24] M. Galimberti, G. Infortuna, S. Guerra, V. Barbera, S. Agnelli, S. Pandini, *Rubber World* **2018**, *5*, 24.
- [25] V. Barbera, A. Citterio, M. Galimberti, G. Leonardi, R. Sebastiano, S. Shisodia, A. Valerio, US10329253B2, **2019**.
- [26] V. Barbera, A. Bernardi, A. Palazzolo, A. Rosengart, L. Brambilla, M. Galimberti, *Pure Appl. Chem.* **2018**, *90*, 253.
- [27] M. Galimberti, V. Barbera, A. Citterio, R. Sebastiano, A. Truscillo, A. M. Valerio, L. Conzatti, R. Mendichi, *Polymer* **2015**, *63*, 62.
- [28] V. Barbera, S. Musto, A. Citterio, L. Conzatti, M. Galimberti, *Express Polym. Lett.* **2016**, *10*, 548.
- [29] M. Galimberti, V. Barbera, A. Truscillo, R. Sebastiano, A. Valerio, EP3180379A1, **2018**.
- [30] V. Barbera, L. Brambilla, A. Milani, A. Palazzolo, C. Castiglioni, A. Vitale, R. Bongiovanni, M. Galimberti, *Nanomaterials* **2018**, *9*, 44.
- [31] M. Galimberti, V. Barbera, R. Sebastiano, A. Valerio, G. Leonardi, A. Citterio, US10160652B2, **2018**.
- [32] D. Locatelli, V. Barbera, L. Brambilla, C. Castiglioni, A. Sironi, M. Galimberti, *Nanomaterials* **2020**, *10*, 1176.
- [33] S. Guerra, V. Barbera, A. Vitale, R. Bongiovanni, A. Serafini, L. Conzatti, L. Brambilla, M. Galimberti, *Materials* **2019**, *13*, 39.
- [34] A. L. Window, in *Strain Gauge Technology*, Springer, The Netherlands **1992**.
- [35] D. Raiteri, M. Saalmink, M. Burghoorn, P. Zalar, M. Martemucci, M. van de Walle, P. Berben, E. Smits, in *2019 IEEE Sensors*, IEEE, Piscataway, NJ **2019**, pp. 1–4.
- [36] M. M. A. Burghoorn, P. Zalar, J. van den Brand, D. Raiteri, E. C. P. Smits, US20220196492A1, **2020**.
- [37] Tekscan, Embedded Force Sensors, <https://www.tekscan.com/products-solutions/embedded-force-sensors> (accessed: October 2022).
- [38] C. M. A. Ashruf, *Sens. Rev.* **2002**, *22*, 322.
- [39] L. Wang, D. Jones, G. J. Chapman, H. J. Siddle, D. A. Russell, A. Alazmani, P. Culmer, *IEEE Trans. Biomed. Eng.* **2020**, *67*, 1989.
- [40] N. Matsuhisa, H. Sakamoto, T. Yokota, P. Zalar, A. Reuveny, S. Lee, T. Someya, *Adv. Electron. Mater.* **2016**, *2*, 1600259.
- [41] Z. Kappassov, J.-A. Corrales, V. Perdereau, *Rob. Auton. Syst.* **2015**, *74*, 195.
- [42] L. Eisenmann, C. Marschner, Y. Lu, S. Sauer, H. Howard, in *Advanced Microsystems for Automotive Applications*, Springer Berlin Heidelberg, Berlin, Heidelberg **2000**, pp. 147–155.
- [43] V. Barbera, L. Rubino, F. Margani, M. Galimberti, P. Zalar, IT102022000013486, **2022**.